On a model-based control of a three-way catalytic converter

SAE TECHNICAL PAPER SERIES

2001-01-0937

On a Model-based Control of a Three-way Catalytic Converter

M. Balenovic, A. C. P. M. Backx and J. H. B. J. Hoebink
Eindhoven University of Technology

Reprinted From: Emission Control Modeling (SP–1605)

SAE The Engineering Society For Advancing Mobility Land Sea Air and Space® INTERNATIONAL

**SAE 2001 World Congress
Detroit, Michigan
March 5-8, 2001**

ISSN 0148-7191

Printed in USA

2001-01-0937

On a Model-Based Control of a Three-Way Catalytic Converter

M. Balenovic, A. C. P. M. Backx and J. H. B. J. Hoebink
Eindhoven University of Technology

ABSTRACT

Though very important for the system performance, the dynamic behavior of the catalytic converter has mainly been neglected in the design of exhaust emission control systems. Since the major dynamic effects stem from the oxygen storage capabilities of the catalytic converter, a novel model-based control scheme, with the explicit control of the converter's oxygen storage level is proposed. The controlled variable cannot be measured, so it has to be predicted by an on-line running model (inferential sensor). The model accuracy and adaptability are therefore crucial. A simple algorithm for the model parameter identification is developed. All tests are performed on a previously developed first principle model of the catalytic converter so that the controller effectiveness and performance can clearly be observed.

INTRODUCTION

The catalytic converters have become very advanced in the last 25 years in order to push the limits of the exhaust gas purification as far as possible. These limits cannot be achieved, however, without an accurate engine control system, which keeps the input to the converter at the optimal level (stoichiometry). Though quite effective, those control systems do not consider the converter's dynamic behavior, which is not negligible [1,2,3]. This dynamics stems mostly from the oxygen storage capabilities of ceria, which is placed in the washcoat of the catalytic converter. A further improvement of the converter's performance could be achieved if its dynamics is taken into account in the control system. However, mainly due to the complexity and even unfamiliarity with the dynamic processes taking place inside the catalytic converter this latter approach has not often been used. Shafai et al. [4] have shown that it is possible to develop a true catalytic converter controller by controlling the oxygen level stored on ceria in an adaptive way. Though quite effective the proposed scheme has a small drawback in the simplicity of the used converter model, which might also affect the controller performance when a larger dynamic range is considered.

The dynamic effects taking place inside of the catalytic converter can efficiently be studied by developing a converter model. Most models are assuming steady state kinetic submodels coupled by submodels accounting for the dynamic effects induced by the oxygen storage mechanism [5,6,7]. Somewhat more complex are the models that use elementary step kinetics [8,9], but they can provide more complete information on the converter's dynamics accounting also for the dynamics of the noble metal surface. Typically resulting in a set of PDE's that can then be transferred into a larger set of ODE's, these models cannot directly be used for the control. They can, however, provide a useful tool for studying the converter dynamics and initial testing of developed controllers. Another type of recently emerging models is a control-oriented model, mostly based on the storage dynamics [10,11]. These models have less parameters, which can be adapted on-line, they do not impose numeric difficulties and can effectively be used for on-board control and diagnosis. Having less parameters they may have problems to describe a wider dynamic operating range, which requires more frequent parameter adaptation.

This paper presents an approach, which combines the two modeling methods in a theoretic development and testing of a catalytic converter controller. The previously developed first principle model, based on elementary step kinetics, has been used as the basis for the development of a simplified control-oriented model. Since the latter model is used on-line as the inferential sensor for estimation of the level of ceria coverage by oxygen, the model accuracy in a wide dynamic range is crucial. A simple algorithm for the parameter adaptation is developed. Based on the first principle model, dependencies of the parameters on fast changing variables (space velocity, inlet lambda levels) are found which increase the range of the model application. The influence of the converter temperature on the model parameters is also analyzed. The cascade control system consists of the outer loop being the inferential converter controller and the inner loop, which is the standard air-fuel ratio engine controller. The controller performance has been tested on the exhaust system

model consisting of the first principle converter model and an engine model.

FIRST PRINCIPLE CONVERTER MODEL

The first principle model is the basis for the analysis presented in this paper. The model is based on the elementary step kinetics in order to get a fully dynamic model of the converter. The components used to represent the exhaust gas are carbon monoxide, hydrocarbons (ethylene and acetylene), oxygen, nitric oxide, carbon dioxide and water. Hydrogen has not been explicitly modeled, but accounted for by increasing the reaction enthalpy of the carbon monoxide oxidation. Acetylene and ethylene are representatives of slow and fast oxidizing hydrocarbons, respectively. Acetylene is very important at low temperatures because it is known to increase the light-off temperatures of other components by surface inhibition [12,13].

The complete detailed description of the model equations can be found in [8,9], while the used elementary steps are given in appendix. Therefore, the model is only briefly presented here. The monolithic reactor is modeled as a one-dimensional adiabatic reactor with one channel being the representative for the whole reactor. Physical parameters of the reactor are given in table 1. The reactor model is a set of nonlinear partial differential equations for the species in the bulk gas and solid phase as well as adsorbed on the noble metal or ceria surface, and energy equations in the gas and solid phase. Hence the set of PDE-s to be solved is as follows:

$$\frac{\partial}{\partial t}\begin{pmatrix} C_{f,i} \\ C_{s,i} \\ \theta_i \\ T_f \\ T_s \end{pmatrix} = \mathbf{f}\left(\Phi_m^{\sup}, C_{f,i}, C_{s,i}, \theta_i, T_f, T_s, \frac{\partial C_{f,i}}{\partial x}, \frac{\partial T_f}{\partial x}, \frac{\partial^2 T_s}{\partial x^2} \right) \quad (1)$$

The problem is transferred into a larger set of ODE-s by discretization in the axial direction, which is then solved using Backward Differentiation Formulae with variable order and variable size [14].

The kinetic model is defined by the reaction mechanism and corresponding rates for various adsorption, desorption and reaction processes. The submodels for oxidation of carbon monoxide and hydrocarbons have been obtained by transient kinetic experiments on a single Pt/Rh/γ-Al_2O_3/CeO_2 catalyst [13,15,16]. Since the NO reduction model for the same catalyst is unavailable, a model from the literature [17] has been used instead. The latter is rather simple, not accounting for some important processes such as the creation of NO_2 and N_2O species and the interaction of NO species with the ceria surface.

Table 1. Physical parameters of the simulated reactor.

Substrate length	15 cm
Substrate width	10 cm
Cell density	400 cpsi
Wall thickness	$1.7\ 10^{-4}$ cm
Washcoat loading	250 g/L
Washcoat surface area	$1.24\ 10^{4}\ m^2_{cat} m^{-3}_{reactor}$
Noble metal capacity	$2.7\ 10^{-5} mol\ m^{-2}_{cat}$
Oxygen storage capacity	$2.5\ 10^{-3} mol\ m^{-2}_{cat}$

The NO reduction kinetic parameters have been adapted for the converter model to predict the measured emissions during an Euro test cycle [18].

Though quite complex, such a model can give a good insight into dynamic processes occurring inside of the reactor at various operating conditions. The light-off process is predominantly influenced by the noble metal surface dynamics. Acetylene and nitrogen containing species strongly adsorb on the noble metal at low temperatures, so their light-off characteristics determine the overall converter light-off behavior. These modeling results are in line with measured data [7]. Various inlet lambda signal shapes cannot significantly influence the light-off, apart from the ethylene light-off temperature which can be lowered by oscillating the inlet feed [19]. Ceria, with its oxygen storage capabilities, does not have a great influence on the light-off. However, it can slightly promote the CO oxidation by providing necessary oxygen, as oxygen has difficulties to reach the noble metal surface with inhibiting species present. After the light-off the main dynamic effect comes from the oxygen storage and release by ceria. When the inlet feed is lean the excess oxygen is stored on the ceria surface, while it can be released for the reaction with CO and hydrocarbons when the inlet feed turns to rich. Partially empty ceria surface also promotes the NO reduction. Even without a direct interaction of NO with ceria modeled, NO reduction is enhanced when the ceria surface is not completely filled: NO can adsorb and dissociate on the empty noble metal surface while oxygen fills the ceria surface. The range of high conversion is thus broadened under the dynamic operation of the converter.

Modeling results are in good agreement with measured converter dynamics [1,2,3], though the latter was obtained at higher temperatures. These experiments have shown that the converter exhibits a substantial dynamic behavior with the rich inlet feed after the ceria surface has been emptied. This is assigned to water gas

shift and steam reforming reactions, which were not modeled in the present study because no elementary step kinetic model is available. This omission is not very serious because these reactions start to play a significant role at somewhat higher temperatures then considered here, and after oxygen removal from the ceria surface [20]. Since the latter is the condition that should be avoided during the converter operation, ceria related dynamics is the most important to be considered in the converter control.

MOTIVATION – Figure 1 shows the inlet and outlet concentrations during lambda step tests. The inlet feed is changed from lean (λ=1.04) to rich (λ=0.96) and back to lean. The inlet mass flow is constant and equals 0.015 kg/s. The inlet temperature is kept at 550K and the reactor was preconditioned with the stoichiometric inlet feed so that the temperatures inside of the reactor are considerably higher. Those conditions will hold for most of the simulations presented in this paper. Oxygen storage operation is clearly visible from the CO and hydrocarbon responses after the lean-rich step, and the NO response after the rich-lean step. From the nature of the oxygen storage operation it is clear that by keeping the amount of oxygen stored on the ceria surface at the optimal value one could enhance the conversion of all species under dynamic operating conditions.

There should be enough oxygen for the conversion of carbon monoxide and hydrocarbons if the inlet turns to rich and yet enough free space on the catalytic surface for the NO reduction if the inlet feed becomes lean. An example is presented in table 2. Mean conversions during one period of the inlet lambda oscillation (A=0.02,f=0.67Hz) in cases with initially completely filled, emptied and half filled oxygen storage are given. Note that only with half filled oxygen storage the conversion is 100% in all three cases. Though the oscillations are not very high in amplitude, CO and hydrocarbon conversion significantly drop during the rich half cycle, while NO conversion drops during the lean half cycle. NO conversion predicted by the model should be taken with some reservation because of the simplified kinetic model used. The oxygen storage dynamics should clearly be considered in the emission controller if one wants to obtain a zero emission vehicle.

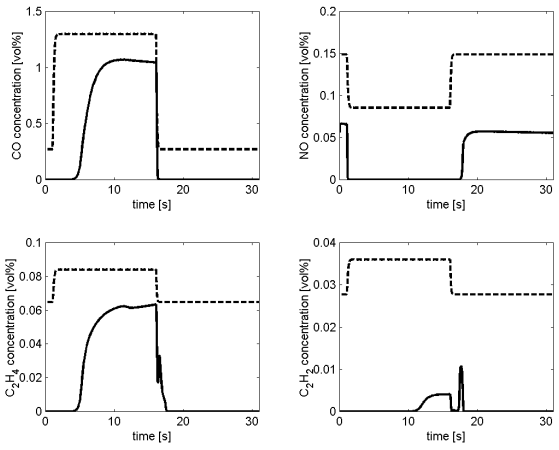

Figure 1 Converter inlet (dashed) and outlet (solid) concentrations during inlet lambda step changes.

Table 2 Conversion during one period of inlet lambda oscillations with different initial conditions.

conversion	CO	HC	NO
empty OSC	81%	77%	100%
medium OSC	100%	100%	100%
full OSC	100%	100%	96%

CONTROL-ORIENTED MODEL

Oxygen storage based models have already been used by some authors to obtain a simple control-oriented model, which could also been used for the on-board diagnostics [10,11]. The model used in this study is in its structure very similar to the model of Brandt et al. [10], but with additional features included to account for the effects of space velocity and inlet signal amplitudes. The effects of temperature variations inside of the reactor will also be addressed. The model basically has to link the measurable inlet and outlet lambda values with the unmeasurable degree of ceria coverage (which will in further text be referred to as the relative oxygen level). The basic model structure is as follows:

$$\frac{d\zeta}{dt} = \frac{1}{k_d}\lambda_{in} f(\zeta), \tag{2}$$

$$\lambda_{out} = \lambda_{in} - k_d \frac{d\zeta}{dt} \tag{3}$$

Both inlet and outlet lambda values are obtained by subtracting 1 from the measured values. In this manner positive lambda values represent lean mixtures, while negative represent rich mixtures. The relative oxygen level (ζ) assumes the values between 0 and 1, where 1 stands for the completely filled oxygen storage and 0 the completely empty oxygen storage. The relative oxygen level is the mean oxygen level throughout the converter, thus approximating the distributed-parameter system with a concentrated-parameter model. The scaling factor, k_d, reflects the total oxygen storage capacity and applied space velocity (proportional to OSC and inversely proportional to space velocity), while the nonlinear function, f(ζ), describes the reaction rate as a function of

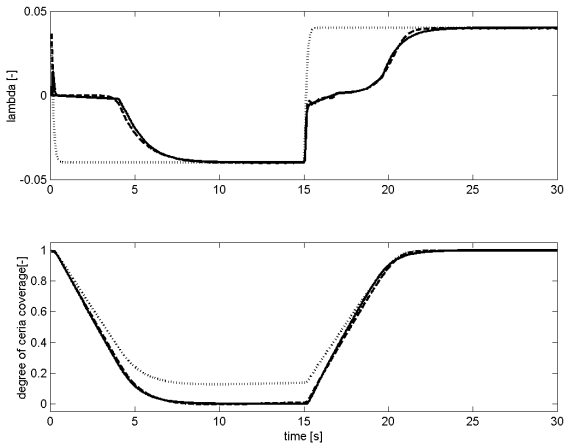

Figure 2 Control-oriented model estimation. Above: inlet lambda (dotted), outlet lambda (dashed), outlet lambda predicted by the control-oriented model (solid). Below: average ceria coverage by oxygen before (dotted) and after rescaling (dashed), and control-oriented model predicted relative oxygen level (solid).

the relative oxygen level. There are actually two functions, one for the lean inputs $f_L(\zeta)$ and one for the rich inputs $f_R(\zeta)$. When it will not be necessary to distinguish between them, $f(\zeta)$ will be used. The model uses an assumption that the relative oxygen level can only be increased with a lean feed and decreased with a rich feed. It also assumes that when the feed becomes stoichiometric the relative oxygen level reaches immediately the steady state. It will be shown in the text that these assumptions are not completely correct and lead to small errors, but the model simplicity, however, remains a strong advantage for such an approach.

PARAMETER ESTIMATION – Since the catalytic converter changes its behavior with time, i.e. ages, the model parameters should be adapted on-line to the new conditions. Due to the model simplicity a rather simple algorithm can be utilized for the parameter estimation. The estimation needs measured inlet and outlet lambda values from one rich-lean and one lean-rich step. The scaling parameter, k_d, is obtained from one step response by integrating the difference between the inlet and outlet lambda value during the step response:

$$k_d = \int_0^{Ts} (\lambda_{in} - \lambda_{out}) dt \qquad (4)$$

There is a small difference between the parameters, when calculated from a lean or a rich step (around 5%). This is the result of a slight nonlinearity of the lambda function. When the oxygen storage capacity is known, the reaction rate function, $f(\zeta)$, can be calculated by combining equations 2 and 3:

$$\frac{d\zeta}{dt} = \frac{1}{k_d}(\lambda_{in} - \lambda_{out}), \qquad f(\zeta) = 1 - \frac{\lambda_{out}}{\lambda_{in}} \qquad (5)$$

The algorithm can easily be transferred into the discrete domain to be used on a digital computer. Since there is no recursion in the algorithm, this is in fact an off-line algorithm, which due to its simplicity can be applied on-line after all the data has been collected.

The comparison of the outlet signals generated by the first principle model and estimated by the simplified model, as presented in figure 2, shows the efficiency of the algorithm. The generated data are taken from the case presented in figure 1. The converter outlet lambda value is calculated from the gas concentrations according to the following relation:

$$\lambda = \frac{2C_{O_2} + C_{NO} + C_{CO} + 2C_{CO_2} + C_{H_2O}}{2C_{CO} + 6C_{C_2H_4} + 5C_{C_2H_2} + 2C_{CO_2} + C_{H_2O}} \qquad (6)$$

The function $f(\zeta)$ is a piecewise linear function so that estimation procedure becomes quite simple. Also the averaged degree of the ceria coverage throughout the reactor is compared with the relative oxygen level calculated by the simplified model (figure 2 below). In order to make a fair comparison the lower bound of the first principle model generated ceria coverage has to be rescaled. The first principle model predicts that the ceria surface is not completely depleted even in the steady state when the inlet feed is rich. This means that there is still a part of ceria covered with oxygen, but this oxygen cannot be used for the oxidation of CO and hydrocarbons. This occurs close to the inlet of the reactor where the temperature is relatively low. Figure 3 shows the washcoat temperature profile and ceria surface coverage by oxygen at the end of the rich step. The inhibiting species, nitrogen containing species and acetylene, occupy most of the noble metal surface close to the reactor inlet and do not allow the other species to adsorb. Oxygen from ceria can thus not be fully utilized. As the surface temperature increases this effect of inactive oxygen storage becomes smaller. By varying the space velocities or inlet lambda amplitudes in the rich region the amount of the unused oxygen from ceria also changes, because the conditions (surface coverage of the inhibiting species) on the noble metal surface become different. These changes are not severe, and will also decrease with increasing temperature, but should be accounted for if a highly accurate model is desired at lower temperatures. The control-oriented model in this study does not account for the influence of the space velocity and inlet lambda amplitude on the inactive oxygen storage. These effects, together with the fact that more ceria becomes available for the adsorption of oxygen, explains the experimentally observed oxygen

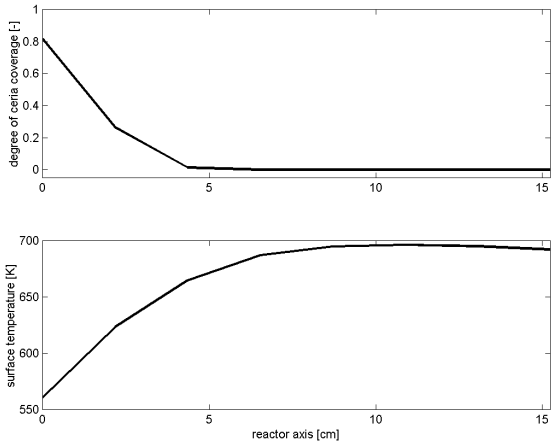

Figure 3 Ceria surface coverage and washcoat temperature profile throughout the reactor at the end of the rich step.

storage capacity increment with increasing temperature [7].

A similar effect can also be observed during the rich-lean step, where the outlet lambda stays rich for some time after the step (see fig. 2). With the empty ceria surface, oxygen easily adsorbs in the front part of the reactor, leaving some components (mostly ethylene) unconverted in the back part of the reactor. This effect is also more important at lower temperatures and also results from the surface inhibition in the front part of the reactor. The model in equation 2 cannot account for this effect, as inlet and outlet lambda values cannot assume different signs. Therefore, the following expression was used to obtain a better fit with the data:

$$\frac{d\zeta}{dt} = \frac{1}{k_d}\left(\lambda_{in} f(\zeta) + g(T)\left(1 - \frac{\zeta}{\zeta_o}\right)\right), \quad if \begin{cases} \zeta < \zeta_o, \\ \lambda_{in} > 0 \end{cases} \qquad (7)$$

The parameter adaptation remains very similar. The above mentioned effect is temperature dependent and is modeled by the second part of equation 7: a positive parameter g(T) that decreases with the temperature. Though the underlying kinetic effect is quite nonlinear a linear approximation for g(T) can be used. The influence of the above given effect is not crucial for a wide range model prediction, and thus a possible modeling error will not have a major impact. When the conditions from equation 7 are not satisfied, equation 2 is used in the model. Control-oriented modeling becomes thus much more complicated at low temperatures, as the effects of highly nonlinear surface inhibition processes have to be accounted for.

CHANGES OF OPERATING CONDITIONS – Model parameters are subject to slow changes in time due to the catalyst aging. These changes can be accounted for by periodic parameter adaptation and should not pose a serious problem for the control system. It is more important to account for the fast changing variables such as space velocity, inlet lambda signals of various amplitudes and changing reactor temperatures.

It was experimentally observed that by adapting only the scaling factor, here k_d, the influence of a changing space velocity can not completely be accounted for [11]. Also the function f(ζ) has to be adapted when the space velocity changes. The reason for this comes directly from the underlying kinetics. The adsorption rate of oxygen on the ceria surface at some point in the reactor depends on the oxygen concentration in the washcoat and the fraction of empty ceria surface:

$$r_a = L_{OSC} k_a C_{O_2} (1 - \chi_o) \qquad (8)$$

The reaction rate between oxygen stored on the ceria surface and CO (or hydrocarbon) absorbed on the noble metal surface depends on the latter surface coverage and the fraction of the ceria surface covered by oxygen:

$$r_r = L_{NM} k_r \theta_{CO,HC} \chi_o \qquad (9)$$

If the function f(ζ) would not be dependant on the space velocity (inlet mass flow) it would mean that for a given relative oxygen level the conversion would not change with a changed mass flow (see equation 5). So, if the mass flow increases with some factor, the reaction rate would also have to increase with the same factor to retain the same conversion. Provided that the analysis of a single reactor point can be applied to the complete reactor behavior, and that the noble metal surface coverages do not change considerably, ceria coverage has to change with the same factor as the mass flow to retain the same conversion as in the nominal case (see eq. 9). The same reasoning holds for the oxygen adsorption on the ceria surface. If the inlet lambda signal amplitude changes from the nominal value (the value at which the estimation was done), the function f(ζ) also has to be adapted in case of a rich inlet. Because the inlet concentrations of reducing components increase with a richer inlet lambda, the reaction rate should also have to increase for the conversion to remain the same. Since this is not the case, $f_R(\zeta)$ has to be adapted for different inlet lambda amplitudes. Because the adsorption rate depends explicitly on the oxygen concentration, $f_L(\zeta)$ does not have to account for the inlet amplitude variations. The model parameters for different operating conditions can therefore be recalculated from the values estimated in a nominal case by simple mapping:

$$k_d = \frac{\dot{m}_{exn}}{\dot{m}_{ex}} k_{dn},$$

$$\zeta_L = 1 - \frac{\dot{m}_{ex}}{\dot{m}_{exn}} + \zeta_{Ln} \frac{\dot{m}_{ex}}{\dot{m}_{exn}}, \qquad (10)$$

$$\zeta_R = \zeta_{Rn} \frac{\dot{m}_{ex}}{\dot{m}_{exn}} \frac{\lambda_{in}}{\lambda_n}.$$

This mapping holds for most of the operating conditions. In some cases, i.e. very high space velocities, it cannot be applied. Both functions, $f_R(\zeta)$ and $f_L(\zeta)$ are piecewise linear and can therefore be represented by set of points $(\zeta, f(\zeta))$. For each point the ζ coordinate is rescaled according to equation 10.

Figure 4 presents the model prediction under the inlet step changes for two times higher and two times lower inlet mass flow in comparison with the nominal case (figure 2). The other conditions have not been changed. Though not perfect, it appears that the above given approximation leads to a reasonably good model prediction under varying operating conditions. Another validation test is shown in figure 5. Various inlet lambda stepwise changes together with inlet mass flow variations are applied. The model prediction is also quite accurate. The largest errors are at low relative oxygen levels because the influence of space velocity and inlet lambda amplitude on the inactive oxygen storage is not completely accounted for. Such an effect is present in the period 25-30s when the inlet feed is only slightly rich and CO has difficulties to reach the noble metal surface and react with the oxygen from ceria, due to relatively low concentration of CO in the feed gas.

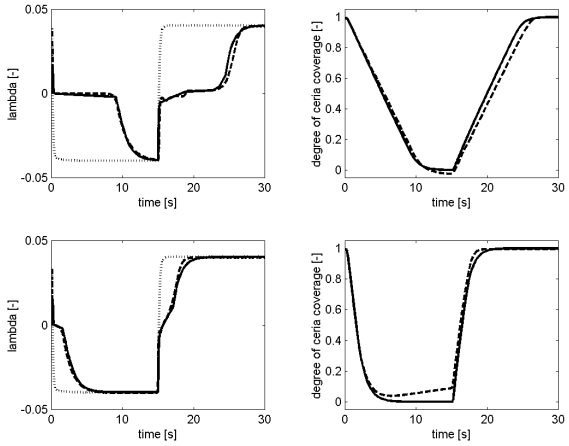

Figure 4 Control-oriented model prediction (solid lines) with two times decreased (above) and two times increased (below) space velocity. The first principle model outputs are given by the dashed lines.

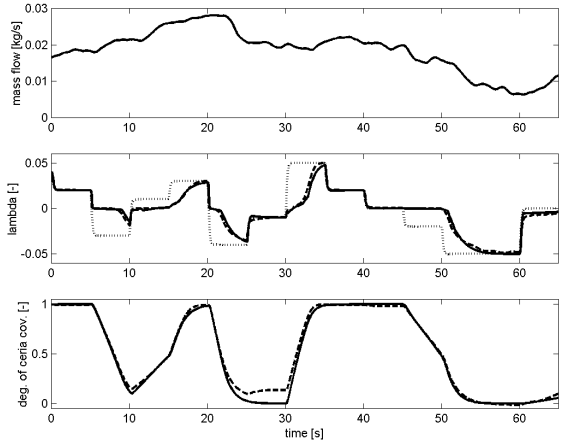

Figure 5 Control oriented model validation with lambda inputs of different amplitudes and with varying mass flow. Dashed lines – the first principle model; solid lines – control oriented model.

MODEL-BASED CONTROLLER

Since the level of oxygen stored on the ceria surface can only be estimated by using the model, an inferential sensor based control system can be applied. The novel control scheme is a cascade system with the inferential oxygen storage controller in the outer loop and a standard model-based air-fuel ratio engine controller in the faster inner loop of the control system, as shown in figure 6.

ENGINE MODELING AND CONTROL – A Mean Value Engine Model [21,22,23] is simple but accurate enough to account for the dynamics important for the air-fuel ratio control. It has therefore been selected to represent the engine dynamics so that the whole exhaust emission control system can be simulated. The model basically consists of two subsystems – the intake manifold and the fuel delivery. The intake manifold subsystem accounts for the air charging and the key equation is the manifold pressure state equation:

$$\dot{p}_m = \frac{RT_m}{V_m}\left(\dot{m}_{at} - \dot{m}_{ap}\right),$$

$$\dot{m}_{at} = f(\alpha, p_m), \qquad (11)$$

$$\dot{m}_{ap} = f(n, p_m).$$

The fuel delivery subsystem accounts for the wall fuel film formation in the manifold and/or port. A part of the injected fuel does not directly enter the cylinder but sticks on the wall and enters the cylinder only after evaporation. This effect is very important to be properly taken into account in the control system if the large excursions of the engine lambda from the desired value are to be avoided during transients. A simple fuel film model is used:

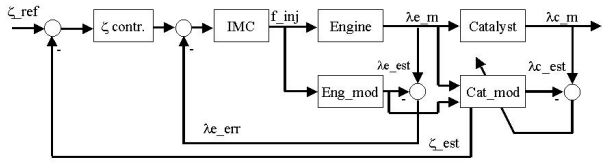

Figure 6 Model-based oxygen storage control scheme.

$$\dot{m}_{ff} = X\,\dot{m}_{fi} - \frac{m_{ff}}{\tau_e},$$

$$\dot{m}_{fc} = \frac{m_{ff}}{\tau_e} + (1-X)\dot{m}_{fi}, \qquad (12)$$

$$X = f(p_m, n), \tau_e = f(p_m, n).$$

With the amount of air and fuel in the cylinder calculated and proper transport phenomena applied, the inlet lambda signal to the catalyst is known.

A perfect estimation of the in-cylinder air is assumed. The engine controller receives the reference lambda value from the catalyst controller. The engine dynamics is faster then the catalyst dynamics and the inner loop therefore much sooner reaches the steady state. The engine controller used in this study is an internal model controller [24]. A characteristic of this controller is the explicit usage of the model, which is run in parallel to the process. The process and model outputs are compared and their difference is fed back to the controller. Note that if the model is perfect the controller is actually a feed-forward controller because the feedback signal equals to zero. It can be shown [24] that if the controller equals to the inverse of the model and the system remains stable, the perfect control would be acquired, i.e. the output lambda would equal the reference lambda signal. Since the wall wetting dynamics is invertible, see (12), the internal model controller is a logical choice. Therefore the inverse of the wall wetting model, coupled with a low pass filter for the improvement of system robustness, is implemented as the engine controller. This system has the predictive advantages of the feed-forward design, but also improved robustness and bandwidth due to the feedback properties.

INFERENTIAL OXYGEN STORAGE CONTROLLER – The outer loop controller calculates the reference lambda signal in order to keep the relative oxygen level at the desired value. Since the relative oxygen level is not measurable, the model, as shown in figure 6, predicts this signal that is than used as a feedback signal. Since the inner closed loop has faster dynamics, it can be assumed that the engine reaches the desired air-fuel ratio instantaneously, i.e. $\lambda_e=\lambda_{ref}$. A possible deviation of the engine air-fuel ratio can be considered as system disturbance. The process delay, which always exists in the path between the fuel injector and the entrance to the catalytic converter, should not be neglected however. Hence the controlled process very much reflects equation 2 and can for one operating point be given by a transfer function in the Laplace domain:

$$G_p(s) = \frac{K_p}{s} e^{-Tds}. \qquad (13)$$

The process gain is highly dependent on the operating conditions, as $K_p=f(\zeta)/k_d$. The controller can assume a very simple P structure:

$$\frac{\lambda_{ref}(s)}{\zeta_{ref}(s) - \zeta_{est}(s)} = \frac{K_c}{T_c s + 1} \qquad (14)$$

Since the model is actually controlled, the controller gain can be adapted in such way that a smooth and fast transition is achieved. The system bandwith is limited by the transport delay, but large amplitudes of the controller output could also cause driveability problems. The controller output (λ_{ref}) is limited in this study between 0.95 and 1.05. The P controller's gain is limited at high frequencies by the low-pass filter to achieve the high frequency noise attenuation. The reference following has a zero steady state offset because of the integrating behavior of the process. The biggest drawback of the P controller is its incapability to remove the steady state error in the presence of system disturbances. Due to the engine controller this problem does not occur as the steady state air-fuel ratio value equals the reference value and thus no steady state disturbance exists.

The controller's reference following and disturbance tracking capabilities are tested. Figure 7 shows the performance of the control system during the tracking of the reference relative oxygen level, which changes from 1 to 0.5. This test resembles the condition after a fuel cut-off when the oxygen storage is filled with oxygen and a fast system response is needed to restore the optimal system performance. The second test presented in figure 8 is the reference tracking from 0 to 0.5. This test can for instance simulate the system performance after a longer period with a rich feed (acceleration), which has completely depleted oxygen from the storage. Again a fast and accurate response is required for a high performance of the system. The reference trajectory is followed quite fast with the system response clearly delayed by presence of the limit on the air-fuel ratio reference value. The model predicted relative oxygen level quite accurately follows the averaged degree of ceria surface coverage predicted by the first principle model used here to simulate the real system. There is a small steady state error in the case presented in figure 8. This is the result of the largest problem imposed by such a control scheme: the actual controlled variable can slowly drift from the desired value due to the integrating process behavior. The outlet error can only be detected by the difference between the converter outlet lambda

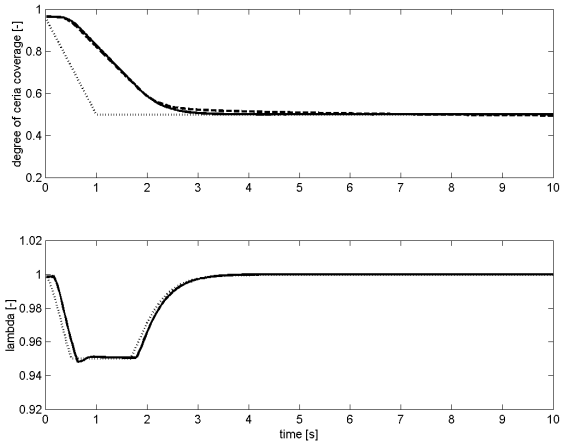

Figure 7 Relative oxygen level reference following during transition from the completely filled to half filled oxygen storage. Above: reference trajectory (dotted), averaged degree of ceria coverage from the first principle model (dashed), and predicted oxygen level by the control-oriented model (solid). Below: lambda reference (dotted) and exhaust lambda (solid).

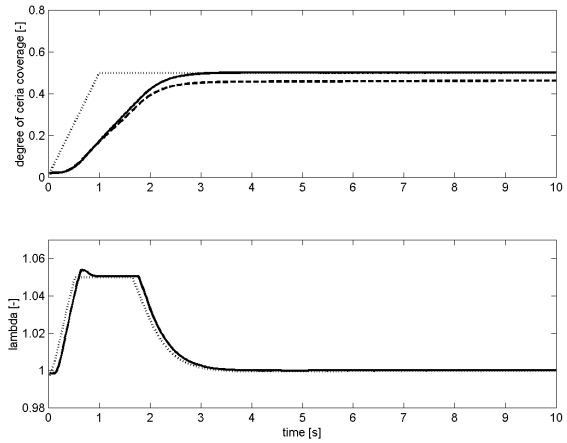

Figure 8 Reference following of the relative oxygen level during transition from the completely emptied to half filled oxygen storage. Signals are the same as in fig. 7.

value and the model predicted outlet lambda value. The controller should also be able to distinguish between the error imposed through disturbances not taken into account (i.e. difference between the measured and actual lambda signal) and errors that occur due to modeling errors. Accurate modeling has therefore a great impact on the control system performance.

Imposing stepwise changes of the throttle, while the relative oxygen level should be maintained on the desired level (here 0.5), tests disturbance rejection capabilities of the controller (figure 9). The control system behavior is fairly good, however with a clear

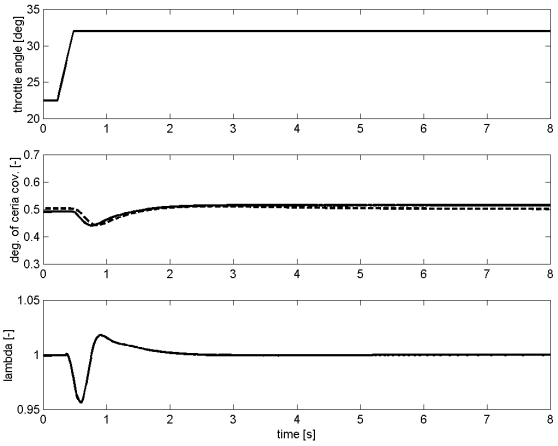

Figure 9 Response of the control system on the disturbance (throttle position) step changes. Above: throttle position. Middle: degree of ceria coverage in the first principle model (solid), and control-oriented model predicted relative oxygen level (dashed). Below: converter inlet lambda signal.

steady state error. This follows not only from modeling errors that were already discussed before, but also from the distributed parameter nature of the catalytic converter. Together with the averaged ceria coverage, the distribution of oxygen throughout the reactor can assume an important role when controlling the relative oxygen level. The current control-oriented model however, does not account for it.

Some very important aspects, such as sensor errors, which commonly occur in the exhaust emission control, have not been taken into account here and are subject of further studies. The influence of the oxygen distribution on the ceria surface throughout the reactor will also be studied further. Due to the integrating nature of the process, sensor or modeling errors can easily lead to a drift of the relative oxygen level away from the desired value. Because of the explicitly available model together with some imposed constraints, a model predictive controller would be a natural solution, but it has to be quite simplified due to its numerical complexity. Improvement of the model and controller adaptation will also be considered in the future.

CONCLUSION

The feasibility of the model-based oxygen storage controller is investigated in the paper. The rigorous, first principle model based on the elementary step kinetics is used as the basis for the development of a simplified, control-oriented model. The latter can be identified with a simple lambda-step test. Relations, based on the underlying kinetics, have been found that can broaden the operating range of the model with respect to various space velocities and inlet lambda signal amplitudes.

A cascade control system, with an engine internal model controller in the inner loop, is used for control of the relative level of oxygen stored on the ceria surface. Since not measurable, the control variable (relative oxygen level) is estimated by the model. Even a quite simple controller can lead to a reasonably good performance of the system, though some aspects of the system sensitivity to sensor errors and improved model adaptation have to be further investigated. The insights in the converter dynamics obtained via first principle modeling prove to be very important for development of the control-oriented model whose accuracy is crucial for the performance of the control system.

NOTATION

C	concentration	[mol m^{-3}_{f}]
T	temperature	[K]
k_d	scaling coefficient	[-]
L_{NM}	noble metal capacity	[mol m^{-2}_{cat}]
L_{OSC}	oxygen storage capacity	[mol m^{-2}_{cat}]
k_a	adsorption rate coefficient	[$m_f^3 mol^{-1} s^{-1}$]
k_r	reaction rate coefficient	[s^{-1}]
r	reaction rate	[mol $m^{-2}_{cat} s^{-1}$]
m	mass	[kg]
p	pressure	[Pa]
n	engine speed	[rpm]
X	wall wetting factor	[-]
K_p, T_d	process model parameters	[-,s]
K_c, T_c	controller parameters	[-,s]

Greek symbols:

θ	noble metal surface coverage	[-]
Φ_m^{sup}	superficial mass flow	[kg $m^{-2}_{reactor} s^{-1}$]
ζ	relative oxygen level	[-]
λ	normalized air-fuel ratio (lambda value)	[-]
χ_O	ceria surf. cover. at some point in the reactor	[-]
α	throttle angle	[deg]
τ_e	evaporation time constant	[s]

Subscripts:

f	bulk gas
s	washcoat
in	converter inlet
out	converter outlet
a	adsorption
r	reaction
ex	exhaust
n	nominal value
m	intake manifold
at	throttle air
ap	port air
fi	fuel injected
ff	fuel film
fc	in cylinder fuel
ref	reference signal
est	estimated signal by a model

REFERENCES

1. Jackson, R.A., Peyton Jones, J.C., Pan, J. and Roberts, J.B., “Chemical Aspects of the Dynamic Performance of a Three-Way Catalyst”, SAE Parep 1999-01-0312,1999.
2. Cornelius, S.J., Collings, N. and Glover, K., “The Role of Oxygen Storage in NO Conversion in Automotive Catalysis”, preprints Congress on Catalysis and Automotive Pollution Control, vol. 1, 91-100, 2000.
3. Germann, H.J., Onder, C.H. and Geering, H.P., “fast Gas Concentration Measurements for Model Validation of catalytic Converters”, SAE Paper 950477, 1995.
4. Shafai, E., Roduner, C. and Geering, H.P., “Indirect Adaptive Control of a Three-Way Catalyst”, SAE Paper 961038, 1996.
5. Koltsakis, G.C., Konstantinidis, P.A. and Stamatelos, A.M., “Development and application range of mathematical models for 3-way catalytic converters”, Appl. Catal. B: Environmental. 12, 161-191, 1997.
6. Oh, S.H. and Cavendish, J.C., “Transients of Monolithic Catalytic Converters: Response to Step Changes in Feedstream Temperature as Related to Controlling Automobile Emissions”, Ind. Eng. Chem. Prod. Res. Dev. 21, 29-37, 1982.
7. Evans, J.M., Ansell, G.P., Brown, C.M., Cox, J.P., Lafyatis, D.S. and Millington, P.J., “Computer Simulation of the FTP Performance of 3-Way Catalysts”, SAE Paper 1999-01-3472, 1999.
8. Nievergeld, A.J.L., v. Selow, E.R., Hoebink, J.H.B.J. and Marin G.B., “Simulation of a catalytic converter of automotive exhaust gas under dynamic conditions”, Stud. Surf. Sc. Catal. 109, 449-458, 1997.
9. Balenovic, M., Nievergeld, A.J.L., Hoebink, J.H.B.J. and Backx, A.C.P.M., “Modeling of an Automotive Exhaust Gas Converter at Low Temperatures Aiming at Control Application”, SAE Paper 1999-01-3623, 1999.
10. Brandt, E.P., Wang, Y. and Grizzle, J.W., “A Simplified 3-way Catalyst Model for Use in On-Board SI Engine Control and Diagnostics”, ASME International Congress and Exposition, Sixth ASME Symposium on advanced Automotive Technologies, 1997.
11. Peyton Jones, J.C., Jackson, R.A., Roberts, J.B. and Bernard, P., “A Simplified Model for the Dynamics of a Three-way Catalytic Converter”, SAE Paper 2000-01-0652, 2000.
12. Mabilon, G., Durand, D. and Courty, Ph., “Inhibition of Post-Combustion Catalysts by Alkynes: A Clue for Understanding their Behaviour under Real Exhaust Conditions”, Stud. Surf. Catal. 96, 775-788, 1995.
13. Harmsen, J.M.A., Hoebink, J.H.B.J. and Schouten, J.C., “Acetylene and carbon monoxide oxidation over a commercial exhaust gas catalyst: transient kinetic

experiments and modelling", Chem. Eng. Sc., submitted December 1999.
14. NAG Fortran Library Manual, mark 15, vol. 1, 1991.
15. Nibbelke, R.H., Nievergeld, A.J.L., Hoebink, J.H.B.J. and Marin G.B., "Development of a Transient kinetic model for the CO Oxydation by O_2 over a Pt/Rh/CeO_2/γ-Al_2O_3 three-way Catalyst", Appl. Catal. B: Environmental 19, 245-259, 1998.
16. Harmsen, J.M.A., Hoebink, J.H.B.J. and Schouten, J.C., "Transient kinetic modelling of the ethylene and carbon monoxide oxidation over a commercial automotive exhaust gas catalyst", Ind. Eng. Chem. Res. 39, 599-609, 2000.
17. Oh, S.H., Fisher, G.B., Carpenter, J.E. and Goodman, D.W., "Comparative Kinetic Studies of CO-O_2 and CO-NO Reactions over Single Crystal and Supported Rhodium Catalysts", J. Catal. 100, 360-376, 1986.
18. Hoebink, J.H.B.J., Harmsen, J.M.A., Balenovic, M., Backx, A.C.P.M. and Schouten, J.C., "Automotive exhaust gas conversion: from elementary step kinetics to prediction of emission dynamics", preprints Congress on Catalysis and Automotive Pollution Control, vol. 1, 225-236, 2000.
19. Balenovic, M., Harmsen, J.M.A., Hoebink, J.H.B.J. and Backx, A.C.P.M., "Low Temperature Dynamic Characteristics of a Three-way Catalytic Converter", submitted to IFAC Workshop on Advances in Automotive Control, Karlsruhe, March, 2001.
20. Whittington, B.I., Jiang, C.J. and Trimm, D.L., "Vehicle exhaust catalysis: I. The relative importance of catalytic oxidation, steam reforming and water-gas shift reactions", Catalysis Today 26, 41-45, 1995.
21. Hendricks, E., Chevalier, A., Jensen, M., Sorenson, S.C., Trumpy, D. and Asik, J., "Modeling of the Intake Manifold Filling Dynamics", SAE Paper 960037, 1996.
22. Aquino, C.F., "Transient A/F Characteristics of the 5 Liter Central Fuel Injection Engine", SAE Paper 810494, 1981.
23. Almkvist, G. and Eriksson, S., "A Study of Air to Fuel Transient Response and Compensation with Different Fuels", SAE Paper 941931, 1994.
24. Morari, M. and Zafiriou, E., "Robust Process Control", Prentice Hall International Editions, 1989.

APPENDIX

Elementary steps used in the first-principle model of a three-way catalytic converter

* is an active site in noble metal, s an oxygen storage site on ceria.

Dimensions: k [$m^3mol^{-1}s^{-1}$], A [s^{-1}], E [$kJmol^{-1}$]. Note: k=Aexp(-E/RT) where the elementary step is an activated process.

	elementary reaction steps										rate coefficients			
1	O_2	+	2*	$\xrightarrow{k_1^f}$	2O*						k_1^f	$1.01\ 10^5$		
2	CO	+	*	$\underset{k_2^b}{\overset{k_2^f}{\rightleftharpoons}}$	CO*						k_2^f	$9\ 10^5$		
											A_2^b	$5.65\ 10^{14}$	E_2^b	113
3	CO*	+	O*	$\xrightarrow{k_3^f}$	CO_2	+	2*				A_3^f	$2.81\ 10^{13}$	E_3^f	96.8
4	CO	+	O*	$\underset{k_4^b}{\overset{k_4^f}{\rightleftharpoons}}$	OCO*						k_4^f	$4.61\ 10^1$		
											A_4^b	$2.48\ 10^2$	E_4^b	20.3
5	OCO*			$\xrightarrow{k_5^f}$	CO_2	+	*				A_5^f	$2.05\ 10^1$	E_5^f	12.1
6	NO	+	*	$\underset{k_6^b}{\overset{k_6^f}{\rightleftharpoons}}$	NO*						k_6^f	$2.58\ 10^6$		
											A_6^b	$2.59\ 10^{14}$	E_6^b	116.9
7	NO*	+	*	$\xrightarrow{k_7^f}$	N*	+	O*				A_7^f	$3.27\ 10^5$	E_7^f	13.82
8	NO*	+	N*	$\xrightarrow{k_8^f}$	N_2	+	O*	+	*		A_8^f	$8.20\ 10^8$	E_8^f	78.5
9	2N*			$\xrightarrow{k_9^f}$	N_2	+	2*				A_9^f	$3\ 10^{10}$	E_9^f	117
10	C_2H_4	+	2*	$\underset{k_{10}^b}{\overset{k_{10}^f}{\rightleftharpoons}}$	C_2H_4**						k_{10}^f	$1.26\ 10^6$		
											A_{10}^b	$3.33\ 10^9$	E_{10}^b	75.46
11	C_2H_4**			$\underset{k_{11}^b}{\overset{k_{11}^f}{\rightleftharpoons}}$	C_2H_4*	+	*				A_{11}^f	$1.36\ 10^9$	E_{11}^f	76.83
											A_{11}^b	$5.39\ 10^4$	E_{11}^b	23.04
12	C_2H_4**	+	6O*	$\xrightarrow{k_{12}^f}$	$2CO_2$	+	$2H_2O$	+	8*		A_{12}^f	$1.06\ 10^{30}$	E_{12}^f	253.7
13	C_2H_4*	+	6O*	$\xrightarrow{k_{13}^f}$	$2CO_2$	+	$2H_2O$	+	7*		A_{13}^f	$3.55\ 10^2$	E_{13}^f	11.26
14	C_2H_4	+	O*	$\underset{k_{14}^b}{\overset{k_{14}^f}{\rightleftharpoons}}$	C_2H_4O*						k_{14}^f	14.7		
											k_{14}^b	$6.0\ 10^{-5}[s^{-1}]$		
15	C_2H_4O*	+	5O*	$\xrightarrow{k_{15}^f}$	$2CO_2$	+	$2H_2O$	+	7*		A_{15}^f	$1.52\ 10^{10}$	E_{15}^f	78.7
16	C_2H_2	+	*	$\underset{k_{16}^b}{\overset{k_{16}^f}{\rightleftharpoons}}$	C_2H_2*						k_{16}^f	$1.04\ 10^7$		
											A_{16}^b	$1.1\ 10^{11}$	E_{16}^b	94
17	C_2H_2*	+	2*	$\underset{k_{17}^b}{\overset{k_{17}^f}{\rightleftharpoons}}$	C_2H_2***						A_{17}^f	$2.5\ 10^9$	E_{17}^f	44.4
											A_{17}^b	$2.27\ 10^{11}$	E_{17}^b	125

18	C_2H_2*	+	3O*	$\xrightarrow{k_{18}^f}$	2CO*	+	H_2O	+	2*		A_{18}^f	$9.35\ 10^{11}$	E_{18}^f	151
19	C_2H_2***	+	3O*	$\xrightarrow{k_{19}^f}$	2CO*	+	H_2O	+	4*		A_{19}^f	$2.25\ 10^{5}$	E_{19}^f	161
20	C_2H_2	+	O*	$\xrightarrow[\xleftarrow{k_{20}^b}]{k_{20}^f}$	C_2H_2O*						k_{20}^f	$5.34\ 10^{2}$		
											k_{20}^b	5.86 [s^{-1}]		
21	C_2H_2O*	+	2O*	$\xrightarrow{k_{21}^f}$	2CO*	+	H_2O	+	*		k_{21}^f	$8.7\ 10^{3}$[s^{-1}]		
22	O_2	+	2s	$\xrightarrow{k_{22}^f}$	2Os						k_{22}^f	$1.11\ 10^{1}$		
23	CO*	+	Os	$\xrightarrow{k_{23}^f}$	CO_2	+	*	+	s		A_{23}^f	$9.62\ 10^{2}$	E_{23}^f	11
24	C_2H_2*	+	3Os	$\xrightarrow{k_{24}^f}$	2CO*	+	H_2O	+	3s		A_{24}^f	$1.76\ 10^{12}$	E_{24}^f	124
25	C_2H_4*	+	6Os	$\xrightarrow{k_{25}^f}$	$2CO_2$	+	$2H_2O$	+	*	+ 6s	A_{25}^f	$1.76\ 10^{12}$	E_{25}^f	134